Response to Reviewer #2 for Manuscript “Contribution of ground ice melting to the expansion of Selin Co (lake) on the Tibetan Plateau”

The manuscript "Contribution of ground ice melting to the expansion of Serling Co lake on the Tibetan Plateau" by Lingxiao Wang et al. is an interesting and original paper that aims to quantify the water volume contribution to the impressive change in water volume of Seling Co lake in Tibet. The work is original as it uses the ground deformation in areas within the watershed and prone to changes in ground ice volume to deduce the water release by ground ice melting. Three years of Sentinel-1 data from end of 2017 to end of 2020 have been processed by multi-temporal InSAR SBAS technique, leading to a decomposition between seasonal deformation associated mainly to freeze-thaw cycles and a three year trend that is mainly interpreted as decadal ice lense melting (for subsidence) or formation (for uplift). In situ core drillings support the existence of ice rich layers or ice lenses at depth between 2 and 8m, where seasonal deformation or pluri-annual subsidence is observed. Interpretation of GPR results also confirm the existence of ice in the same areas.

The paper is overall well written, present new and interesting data and an original way of quantifying the effect of permafrost degradation on lake level change. The endhoreic nature of this watershed area is also allows to test assumptions or models involved in water cycle quantification. It should be accepted for publication after addressing some comments below, that together lead to a major revision.

The authors are very grateful for the valuable comments and suggestions from the reviewer.
Detailed responses and revisions based on the comments are listed below.

InSAR processing and results

Ansari, de Zan et al. have shown that including only **very short temporal baseline interferograms leads to strong biais**, mostly in the form of a pluri annual subsidence. While my experience is that this bias appears mostly in crop areas, and should not be strong in this area of Tibet, it must be shown here that it is not the case (and I really believe that in Tibet you don’t have such biais, or at least that what you see is real). The difficulty here is that freeze-thaw cycles lead to decreased coherence and high fringe gradient, such that interferograms with temporal baseline larger than 2 months are difficult to unwrap. You may find some methodology of how to overcome this in Daout et al., 2017 paper. A stack of numerous 1 year interferograms could also do the trick, provided that you can unwrap them.

Thank you very much for the valuable comments and suggestions.

1) **We tested different interferograms network schemes at the beginning of the work. A stack of numerous 1-year interferograms was also tested.**

According to the statistics on the interferometric coherence of intra-annual interferogram pairs, interferograms during the stable freezing and thawing months (end of Dec, Jan, Feb, Jul, Aug, beginning of Sep) usually have higher coherences than in the other months. Thus, The 1-year-span interferograms were

only conducted during these months to exclude freeze-thaw cycles.

Two interferograms network strategies were compared.

Strategy #1, interferograms were generated by each SAR image with its two sequential acquisitions, which is the scheme used in this study.

Strategy #2, the 1-year-span interferograms were also included, in addition to the regular intra-annual interferograms used in strategy #1.

The following Figure R1 compares the applicability of the above two strategies in constructing interferogram networks. The interferometric coherence is lower in the months experiencing freeze/thaw transitions than in Jan-Feb and Jul-Aug, but it is maintained above an acceptable level (the averaged coherence of each interferogram above 0.7). The study area doesn't face strong decorrelation taking the interferograms network strategy #1.

However, 1-year interferograms have much lower coherence than interferograms experiencing freeze/thaw transitions.

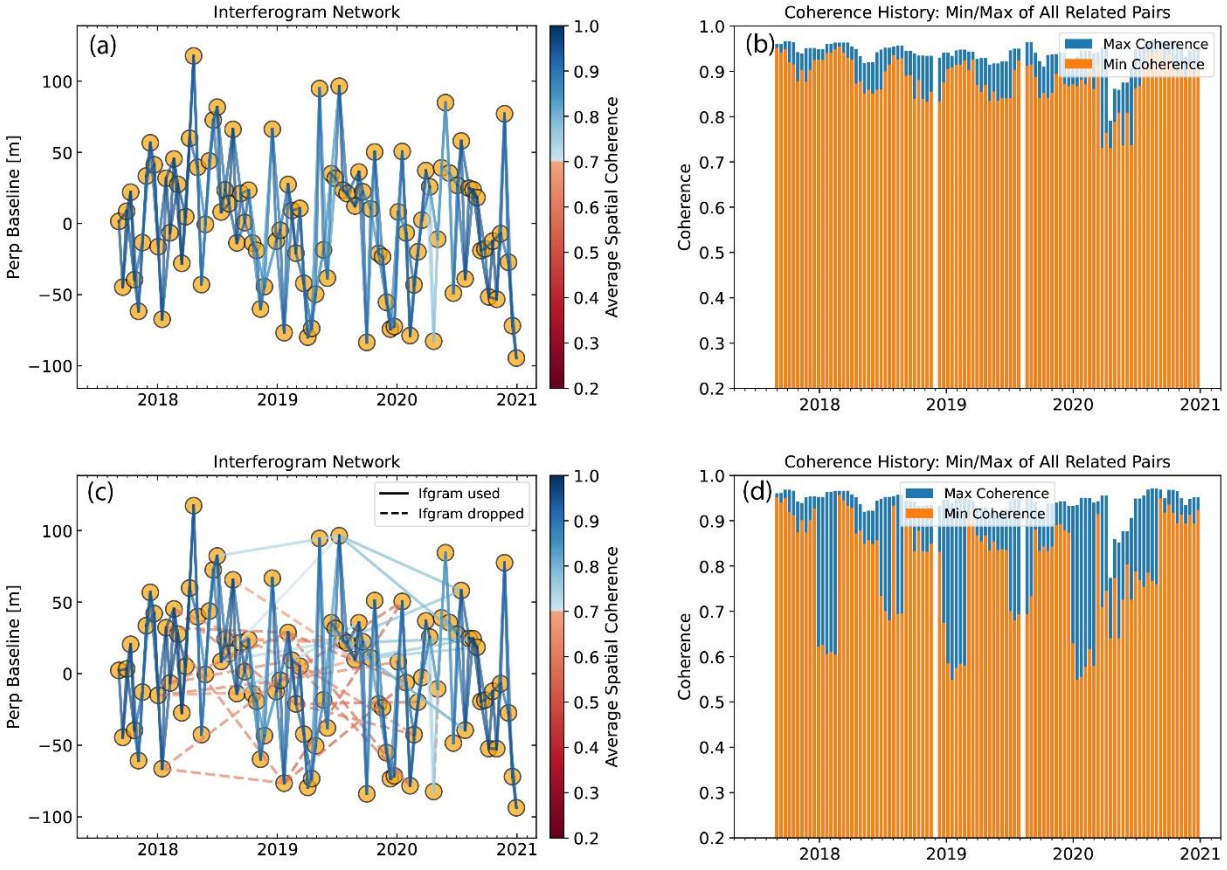

Fig. R1 The upper panel (a-b) shows the interferometric coherence of network strategy #1 and the bottom panel (c-d) shows the results of strategy #2. The extent of interferograms in strategy #2 is slightly smaller than that in strategy #1 (The north-south direction is 40 km smaller). The left panel (a)(c) shows the network of interferograms for deformation time series estimation, color-coded by the average coherence of the interferograms. Circles represent the acquisition dates, and lines represent the interferograms. Solid lines are the interferograms used for time-series estimation, and dashed lines are the interferograms ignored in the time-series estimation. The left panel (b)(d) shows the average coherence of all related pairs for each SAR acquisition date.

2) The qualities of interferograms have been visually examined.

Fig. R2 displays fourteen interferograms together with their unwrapped phases in upstream of Zhajiazangbu, where widespread continuous permafrost is present. The interferograms for each month of the year are presented. In addition to 24-days interferograms, it also displays two 1-year interferograms of 20180702-20190709 and 20190122-20200129. Low interferometric coherence on the 1-year pair is accompanied by unwrapping errors. We didn't observe distinct unwrapping errors among the 24-days interferograms in the land regions (excluding water and glacier). Permafrost-induced deformation is clear on several interferograms. The atmospheric distortions are also strongly visible on several interferograms.

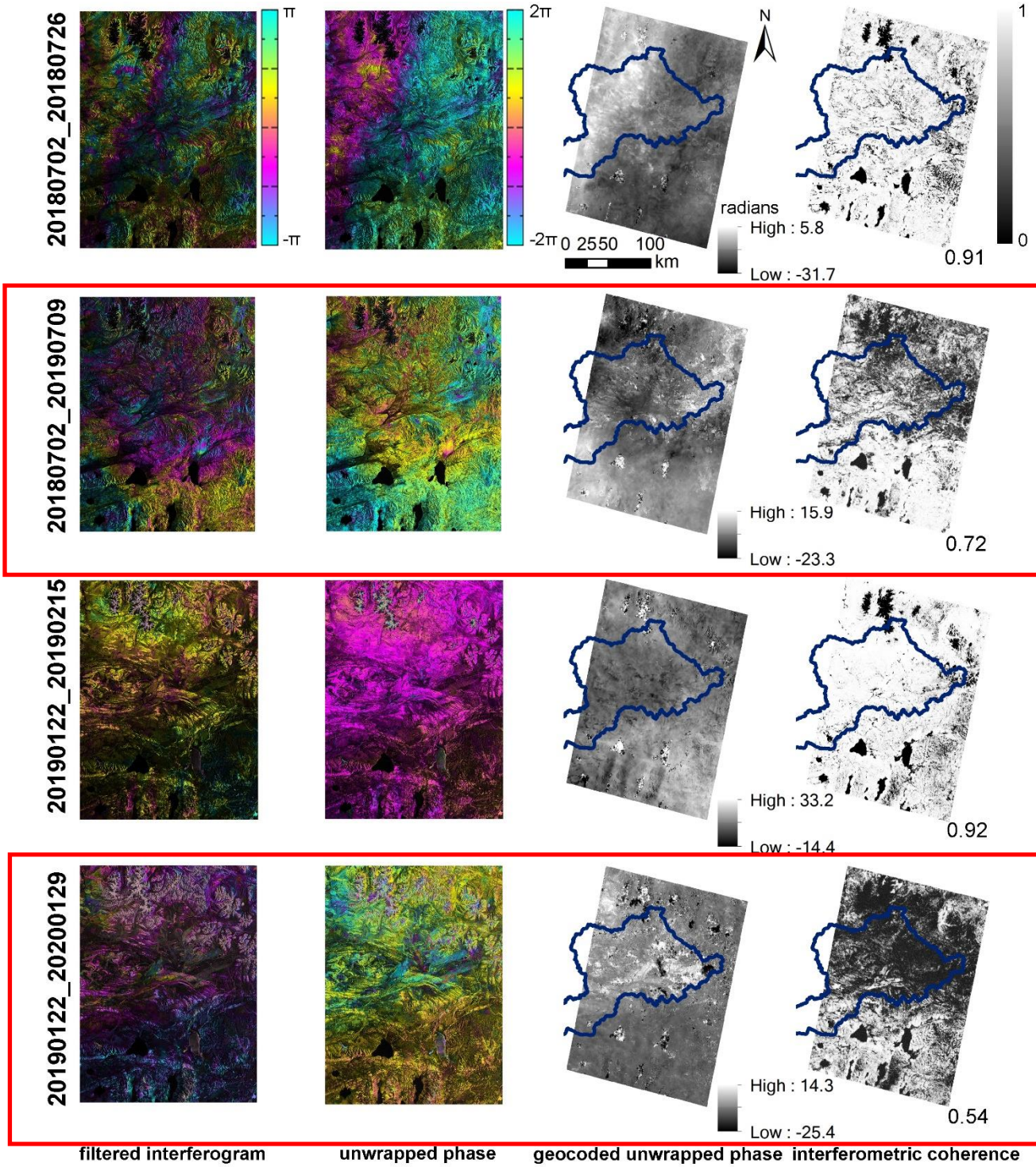

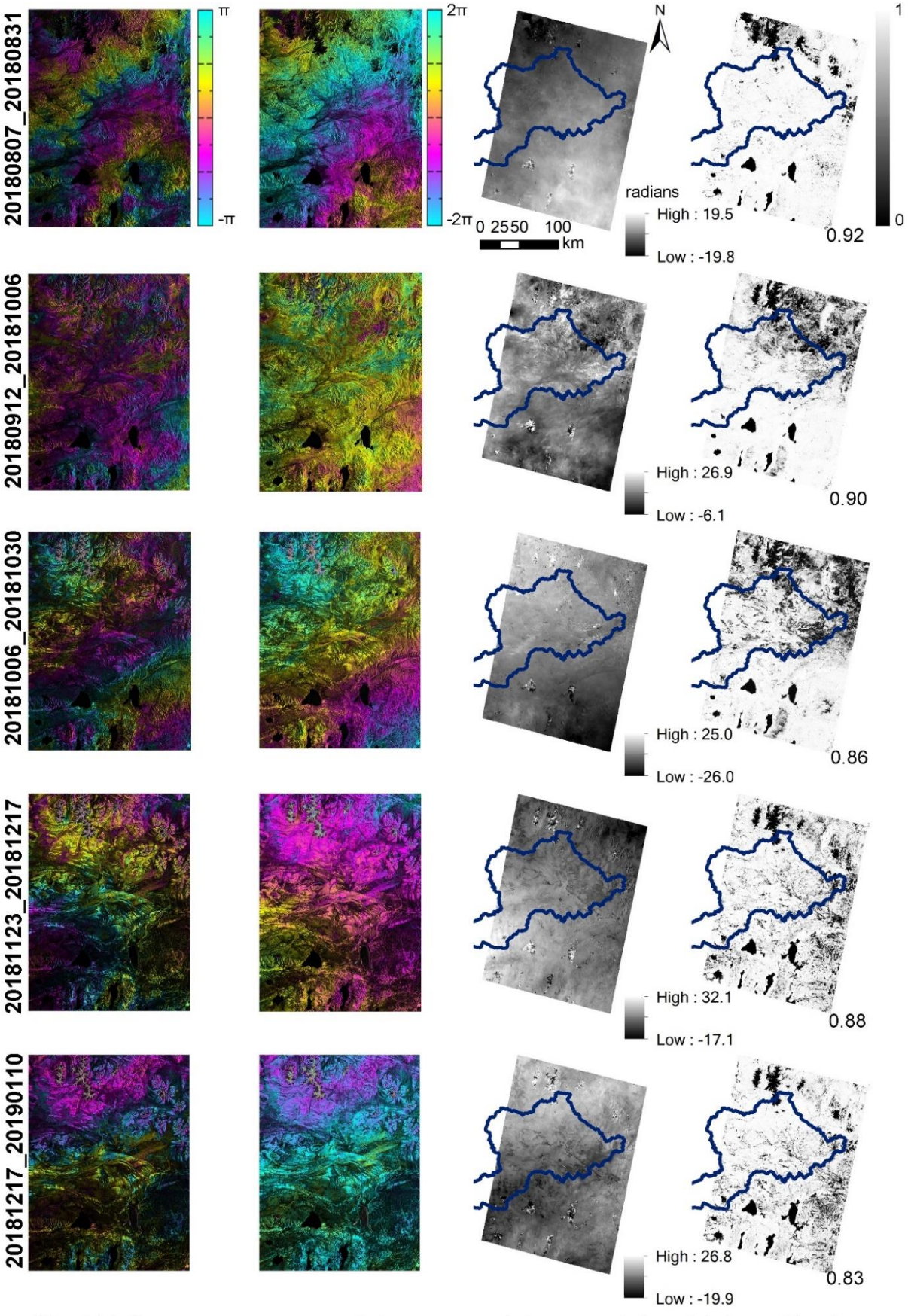
20180807_20180831
π
-π
2π
-2π
N
radians
High : 19.5
Low : -19.8
0 2550 100
km
1
0
0.92
20180912_20181006
High : 26.9
Low : -6.1
0.90
20181006_20181030
High : 25.0
Low : -26.0
0.86
20181123_20181217
High : 32.1
Low : -17.1
0.88
20181217_20190110
High : 26.8
Low : -19.9
0.83
filtered interferogram
unwrapped phase
geocoded unwrapped phase
interferometric coherence

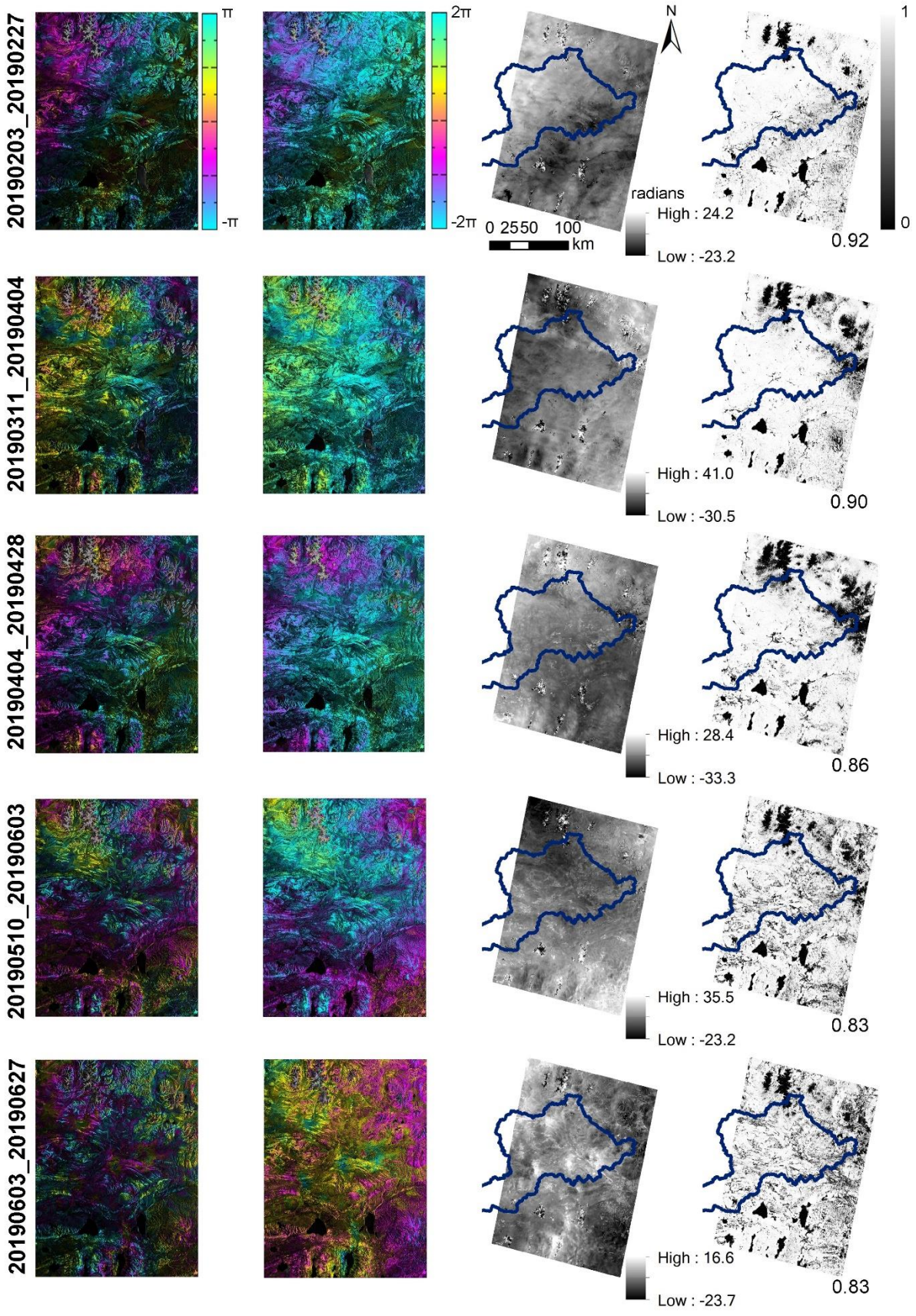

Fig. R2 Examples of 24-days interferograms. The value below the interferometric coherence map labels the averaged value of the map. The decorrelated area in the north is Mt. Geladandong.

3) **The unwrapping error corrections were applied before network inversion to further reduce unwrapping errors (Zhang et al., 2019).** The unwrapping error correction is conducted by bridging reliable regions. The bridging scheme can be described as a three-step procedure for each interferogram. The first step is to identify reliable regions using the connected component information provided by SNAPHU (Chen and Zebker, 2002). The second step is to construct directed bridges to connect all reliable regions using the minimum spanning tree (MST) algorithm minimizing the total bridge length. The third step is to estimate for each bridge the integer-cycle phase offset between the two regions. This is similar to region assembly in the secondary network in phase unwrapping (Chen and Zebker, 2002), but in the tertiary level.

Based on the experiments above, we decided to adopt the scheme that interferograms were generated by each SAR image with its two sequential acquisitions.

Unwrapping: Given the difficulty to unwrap permafrost related InSAR signals, you should show a few examples of 24 days interferograms in an appendix together with their unwrapped counterparts. Can you please use network misclosure (Lopez quiroz et al., 2009) during network inversion to quantify the amount of possible unwrapping error? Please cite the Minimum Cost Flow algorithm used here. The time series shown in the paper, with respect to the reference point quite far away, appear extremely smooth in time, where atmospheric contribution of two points 100km apart should, even in Tibet at its very high elevation, be of at least a cm up to a few cm. Please explain what smoothing you used (I guess embedded in MintPy).

Thank you very much for the valuable suggestion.

1) **The examples of 24 days interferograms are shown in the above Fig. R2.**

2) **Taking the reviewer's suggestion, we also quantitatively evaluate the amount of possible unwrapping error during the network inversion using the idea of network misclosure, but slightly different from (Lopez quiroz et al., 2009).** The methods are stated in section 3.3.1 SBAS-InSAR processing ii) Deformation time series estimation as follows:

Two indicators evaluated the quality of unwrapped phases and inverted raw phase time series: the phase closure of interferogram triplets and temporal coherence. The phase unwrapping algorithms add integer number of 2π phase jumps to recover the unwrapped phase. Interferometric phase noise and discontinuities among different coherent regions may lead to wrong 2π jumps added to the phase field known as unwrapping error. Unwrapping errors can bias the estimated time series. For an interferogram triplet ($\Delta\phi^{ij}$, $\Delta\phi^{jk}$ and $\Delta\phi^{ik}$), unwrapping errors introduce a nonzero integer component C_{int}^{ijk} in the closure phase C^{ijk}. Therefore, the number of interferogram triplets with nonzero integer ambiguity T_{int} can be used to detect unwrapping errors:

$$C^{ijk} = \Delta\varphi^{ij} + \Delta\varphi^{jk} - \Delta\varphi^{ik} \quad (2)$$

$$C_{int}^{ijk} = \frac{C^{ijk} - \mathrm{wrap}\left(C^{ijk}\right)}{2\pi} \quad (3)$$

$$T_{int} = \sum_{i=1}^{T} \left(C_{int}^{ijk}! = 0\right) \quad (4)$$

where $\Delta\varphi^{ij}$, $\Delta\varphi^{jk}$ and $\Delta\varphi^{ik}$ are the three unwrapped interferometric phases generated from the SAR acquisitions at t_i, t_j and t_k, respectively; wrap is an operator that wraps each input number into $[-\pi, \pi)$; and T is the number of interferogram triplets. A triplet without unwrapping errors has $C_{int}^{ijk} \equiv 0$.

The second index, temporal coherence, represents the consistency of the time series with the network of interferograms (Pepe and Lanari, 2006):

$$\gamma_{temp} = \frac{1}{M}\left|H^T \exp\left[j(\Delta\phi - A\widehat{\phi})\right]\right| \quad (5)$$

where (for N SAR images and M interferograms) $\Delta\phi$ is the unwrapped interferometric phase; A is the $M \times (N-1)$ design matrix indicating the acquisition pairs used for interferograms generation (consisting of -1, 0 and 1 for each row with -1 for the reference acquisition, 1 for the secondary acquisition and 0 for all other acquisitions (Berardino et al., 2002)); $\widehat{\phi}$ denotes the estimated time series; H is an M×1 all-ones column vector; and j is the imaginary unit.

Temporal coherence varies from 0 to 1: pixels with values closer to 1 are considered reliable, whereas pixels with values closer to zero are considered unreliable. A threshold of 0.7 is recommended to be used for a dense network of interferograms. In this study, we used a threshold of 0.85; the pixels with temporal coherence below this threshold were masked from the final result.

The quantitative evaluation results are presented in Section 4.4.2 Uncertainties and accuracies of deformation as follows.

Two indicators evaluated the quality of unwrapped phases and inverted raw phase time series: the phase closure of interferogram triplets and temporal coherence. Fig. 11 in the revised manuscript shows the spatial distribution of the number of interferogram triplets with nonzero integer ambiguity T_{int} (Eq(4)), with the histogram illustrating the distribution of T_{int} values within the Selin Co watershed after excluding glaciers and water bodies. The areas having T_{int} smaller than three take part 95% of the watershed, while 72.3% of the watershed has T_{int} value of zero (no wrapping error on all the interferograms). The T_{int} evaluated the quality of original interferometric unwrapped phases, and the unwrapping errors could be further reduced by bridging reliable regions before network revision (Zhang et al., 2019).

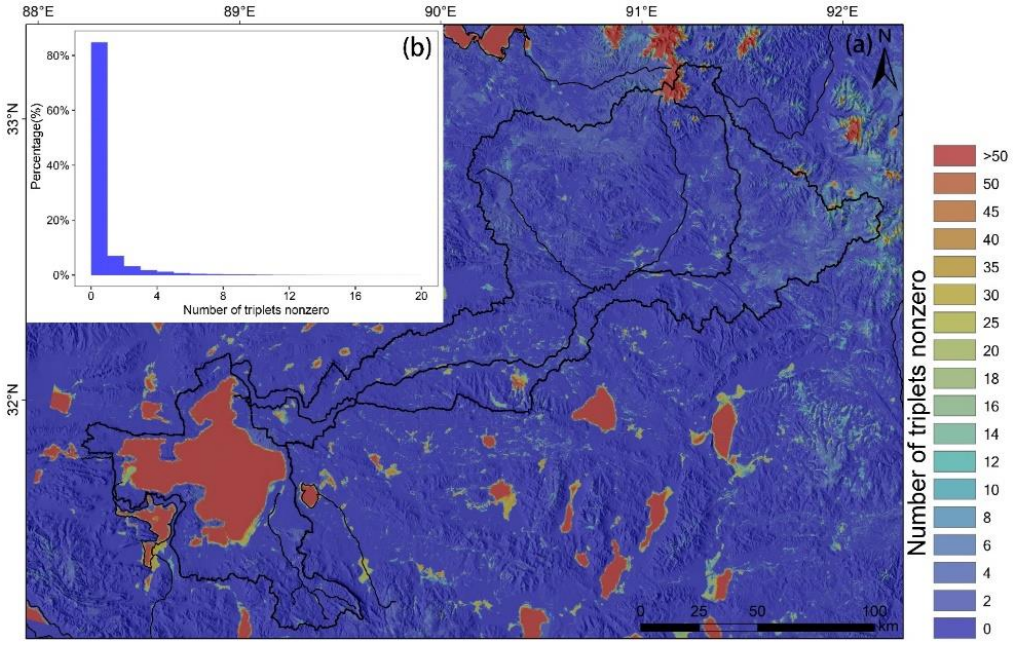

Figure 11 (a) Map of the number of interferogram triplets with nonzero integer ambiguity T_{int} (Eq(4)), (b) histogram illustrating the distribution of T_{int} values within the Selin Co watershed excluding glaciers and water bodies.

Fig. 12 shows the spatial distribution of temporal coherence (Eq.(5)), which is used to evaluate the quality of raw phase time series. 99.0% of the watershed has temporal coherence higher than 0.8, 98.1% has temporal coherence higher than 0.85, 96.0% has temporal coherence higher than 0.9, and 89.1% has temporal coherence higher than 0.95.

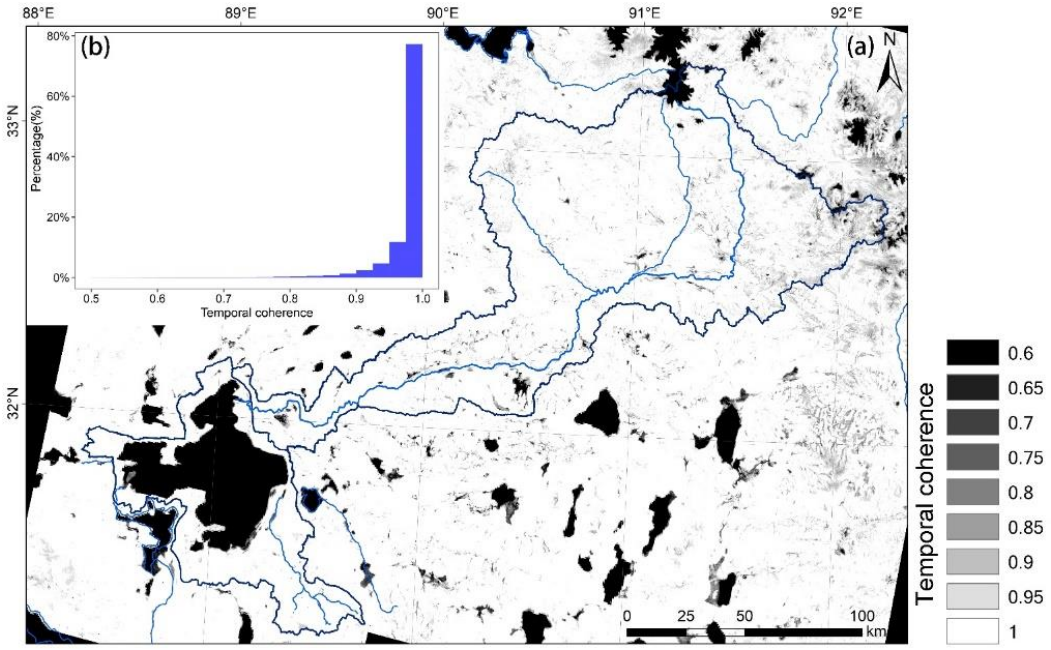

Figure 12 (a) Map of temporal coherence (Eq(5)), (b) histogram illustrating the distribution of temporal coherence values within the Selin Co watershed excluding glaciers and water bodies.

3) **The Minimum Cost Flow algorithm has been cited in the revised manuscript.** It has been cited in the revised manuscript that "To unwrap the differential phase, the SNAPHU Minimum Cost Flow (MCF)

phase unwrapping algorithm (Chen and Zebker, 2002) was applied."

4) **Regarding the selection of reference point and residual atmospheric distortions**, we realized that it is inappropriate to put it such far away from the studying watershed giving consideration to atmospheric distortions and tectonic movements on the TP. We selected a reference point near the boundary of Selin Co watershed not affected by permafrost in dry and flat terrain. The residual phases from atmospheric distortions and tectonic movements on the TP are difficult to remove completely in such a large-scale extent. However, the effect could be reduced by setting the reference near the study area. Taking several helpful suggestions of the reviewer, we have reprocessed the SBAS network inversion. After this reprocessing, the residual distortions (e.g., large area of slight uplift in the previous manuscript) have been reduced, or at least reduced in the studying watershed. The results are correspondingly updated through the revised manuscript.

5) **The time series appear smooth because we applied a 3-size moving window filter to the deformation time series.** We stated that "To minimize the effects of extreme values, we also applied a 3-size moving window filter to the deformation time series." in the section "3.3.2 Extraction of the periodic (seasonal) amplitude and long-term rate" in the original manuscript. To be clear, we have moved this sentence to the end of section "3.3.1 SBAS-InSAR processing" in the revised manuscript. The following Fig. R3 shows the deformation time series of drilling sites before (small black dots) and after (large green dots) 3-size moving window filtering.

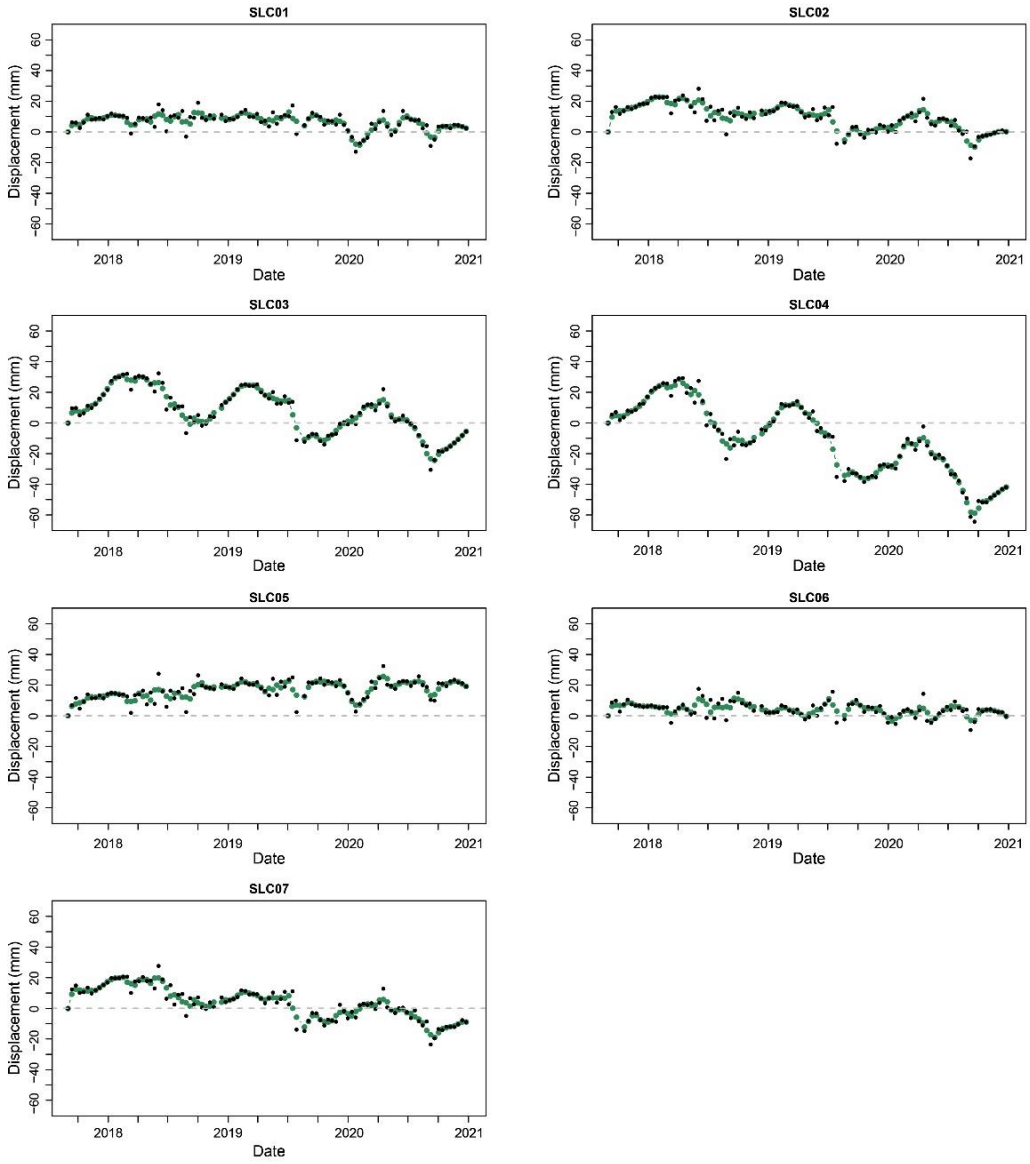

Fig. R3 Deformation time series of drilling sites before (small black dots) and after (large green dots) 3-size moving window filtering.

The discussion of possible **uplift and hence permafrost aggradatio**n could be improved. First of all, one can see on Figure 6 an E-W and N-S trend in velocity in areas not affected by permafrost, the trend resulting in apparent uplift on the NE corner. Deramping here should be evaluated on pixels not affected by permafrost (otherwise the ramp that is removed is affected by subsidence). A display of the seasonal amplitude and velocity field of the whole study area could help assess this trend. On Fig5, inserting panels with zooms on the amplitude and trend plus the location of time series would help the reader. The patterns associated with uplift could then be visualized in correspondence with the optical image. If the uplift is due to permafrost aggradation, it should also have a seasonal component as ice freezing only happens in winter/spring. Please note that sedimentation cannot lead to uplift, as it only destroys coherence. InSAR only follows the displacement of targets that remain coherent between successive acquisitions.

Thank you very much for the valuable advice. Taking several helpful suggestions from the reviewer, we have

reprocessed the SBAS network inversion. We have also selected a larger sector and part of which is covered by both orbit 150 and orbit 48, to assure that the deformation pattern appears on both of the results from the two tracks. Taking the reviewer's suggestion, the zoomed seasonal amplitude and velocity are displayed along with an optical image and DEM overlapped on the hill shade for a better interpretation of the results. The locations of the sites are labeled on all the subfigures. These sites all have high interferometric coherence and T_{int} value of zero (no wrapping error on all the interferograms). Due to a lack of field investigation, it is hard to attribute it absolutely to permafrost aggradation or the rise of the groundwater table or sedimentation. Thus, we only presented the uplift signal and discussed this phenomenon in the discussion section in the revised manuscript.

The discussion of the uplift signal has been adjusted and moved to section "5.1 Uplift displacement signal" as follows.

5.1 Uplift displacement signal

In addition to widespread subsidence detected in upstream of Zhajiazangbu of the continuous permafrost environment, the uplift signal was also observed in the sporadic permafrost environment in the middle stream of the Zhajiazangbu subbasin, also near some drained ponds. Fig. 13 shows a sector (location marked in red rectangle in Fig. 1, 6–7), in which both subsidence and uplift signals are detected. The mean annual air temperature is -2.0°C, calculated based on ERA5-Land air temperature hourly reanalysis data during 2017–2020. For a better interpretation, Landsat optical image and elevation overlapped on the hillshade were also presented. The spatial distribution pattern of deformation aligns with landscape and topography very well. Large seasonal amplitude only appears in the vegetated and wet area, which indicates the water storage in the active layer in a certain way. Uplift signals are generally at the slope feet. Fig. 13(e)–(h) displays the deformation time series of four sites s1-s4 from high elevation to low elevation. Site s2 is stable, viewing from seasonal amplitude and long-term deformation velocity. The subsidence of site s3 is the result of ground ice melting, confirmed by the large periodic seasonal amplitude caused by frost heave and thaw subsidence in the active layer. The uplift signals of site s1 and site 4 are worth exploring, especially site s4. Site s4 has a possibility of being related to ground ice aggradation since it also exhibits moderate seasonal amplitude, but it is more likely related to sediment accumulation or groundwater table rise regarding its location.

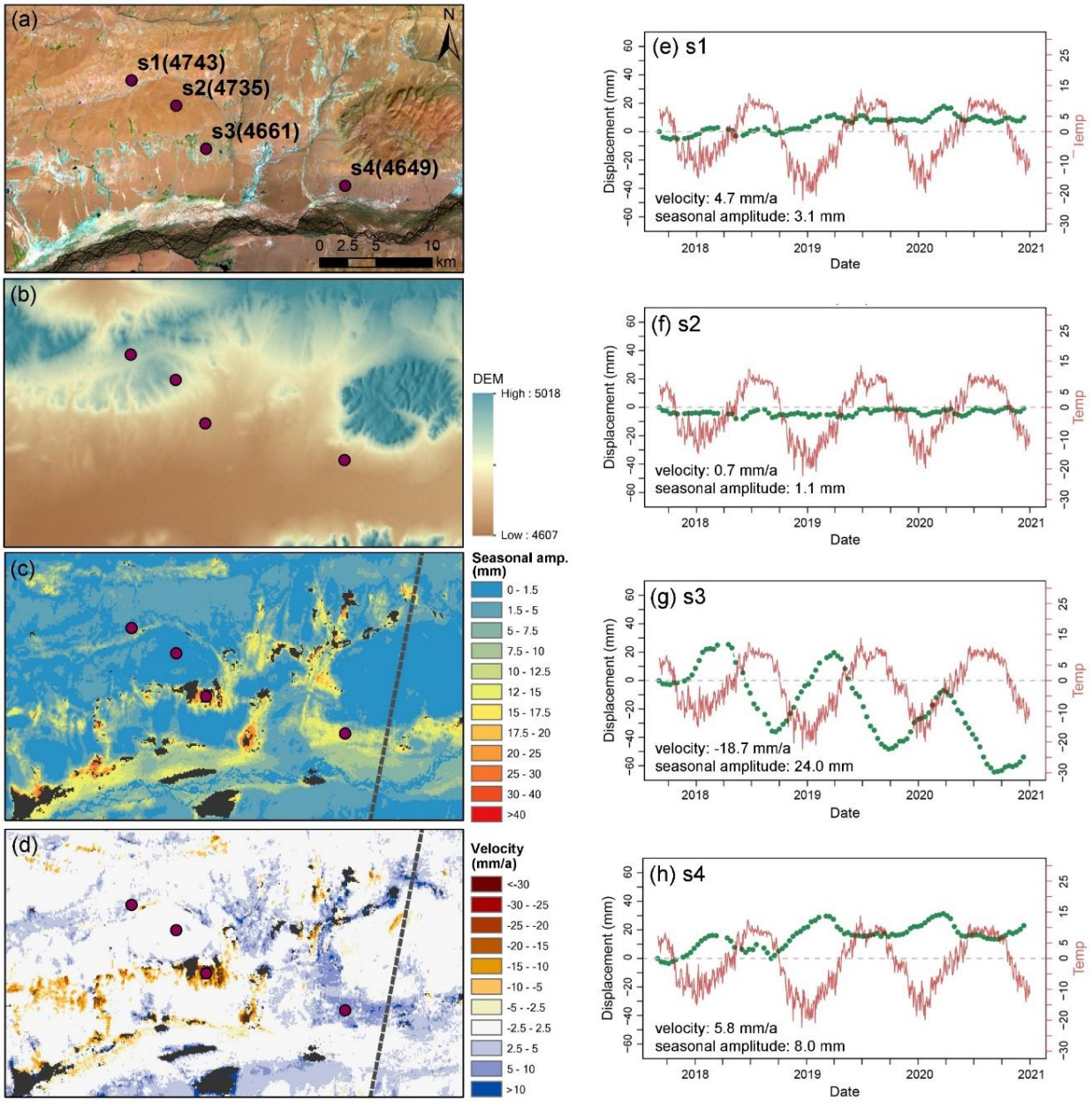

Figure 13 Deformation characters. The sector is marked with the red rectangle in Fig. 1 and 7-8. (a) Landsat 8 image (red: SWIR1, green: NIR, blue: red). (b) DEM overlapped on the hillshade, which is calculated using DEM with the Sentinel-1 incidence angle and azimuth angle. (c)(d) are seasonal deformation amplitude and long-term deformation velocity, respectively. The grey dashed line delineates the track boundary of orbit 150. (e)-(h) are deformation time series of marked sites. Air temperature in red color is from ERA5-Land air temperature reanalysis data. Deformations are in the LOS direction.

Previous research normally focuses on the thaw subsidence signal on the TP, and less attention has been given to the uplift signal. Some of the uplift signals might be related to deposition or the rise of the groundwater table. Some of the uplift signals might be caused by ground ice aggradation. A sufficient water supply accompanied by strong evaporation (cooling effect, energy is taken away) might facilitate the upward freezing of previously unfrozen (or seasonally frozen) sediment. Ground ice aggradation is slightly surprising in the overall warming climate of the study area. However, the upward freezing of previously unfrozen (or seasonally frozen) sediment is still possible and may occur because of sediment accretion (e.g., deltaic and alluvial sedimentation) (French, 2017). A previous study (Daout et al., 2020) also detected a complex

deformation signal in the permafrost on the northeastern Tibetan Plateau and hypothesized that the uplift deformation in lowland regions was caused by excess meltwater pooling, which triggered an increase in the segregation of ice near the permafrost table. On the TP, new permafrost forming is detected on the exposed bottom of Zonag Lake (Zhang et al., 2022). Thus, on the TP, it might be common for degradation and aggradation of ground ice to both occur in permafrost environments, with degradation representing the dominant pattern and aggradation existing in local areas. Currently, most studies focus on permafrost subsidence signals, and few studies have studied permafrost ground ice aggradation and the causes of uplift signals in local environments. Nevertheless, the uplift signals in the permafrost environment on the Tibetan Plateau are worthy of additional research, and further details on the Selin Co basin are expected to be unveiled and supplemented by the next field survey.

The footprint of the two tracks, the satellite heading and LOS direction should be shown on a figure. Please put also the LOS direction on the amplitude and velocity maps, even if you assume vertical displacement (which is decent here). Please state line 155 if you processing ascending or descending tracks.

Thank you for the suggestion.

1) **The descending tracks were emphasized.** It has been stated in the revised manuscript that "In total, 95 acquisition dates for descending orbit 48 and 100 acquisition dates for descending orbit 150 from September 2017 to December 2020 were processed."

2) **The tracks of orbit 150 and orbit 48 are marked in Fig. 1.**

Appendix Fig. A2 also presented the results from orbit 48 and 150, respectively.

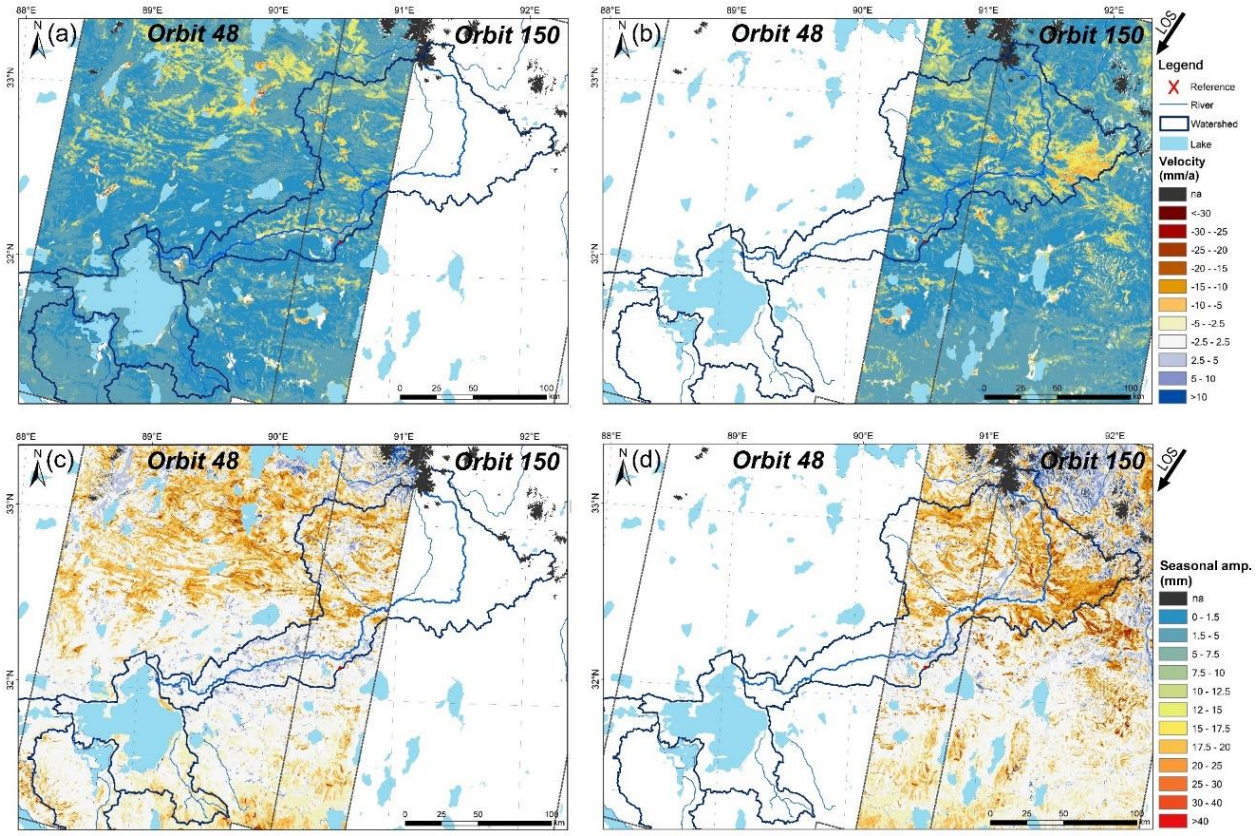

Fig. A2 Map of the periodic (seasonal) amplitude (a)(b) and long-term velocity (c)(d) retrieved from orbit 48 (a)(c) and orbit 150 (b)(d), respectively, all are in the satellite LOS direction.

3) **The satellite heading and LOS direction have been marked** in Figure 6 (seasonal amplitude) and Figure 7 (deformation velocity) in the revised manuscript.

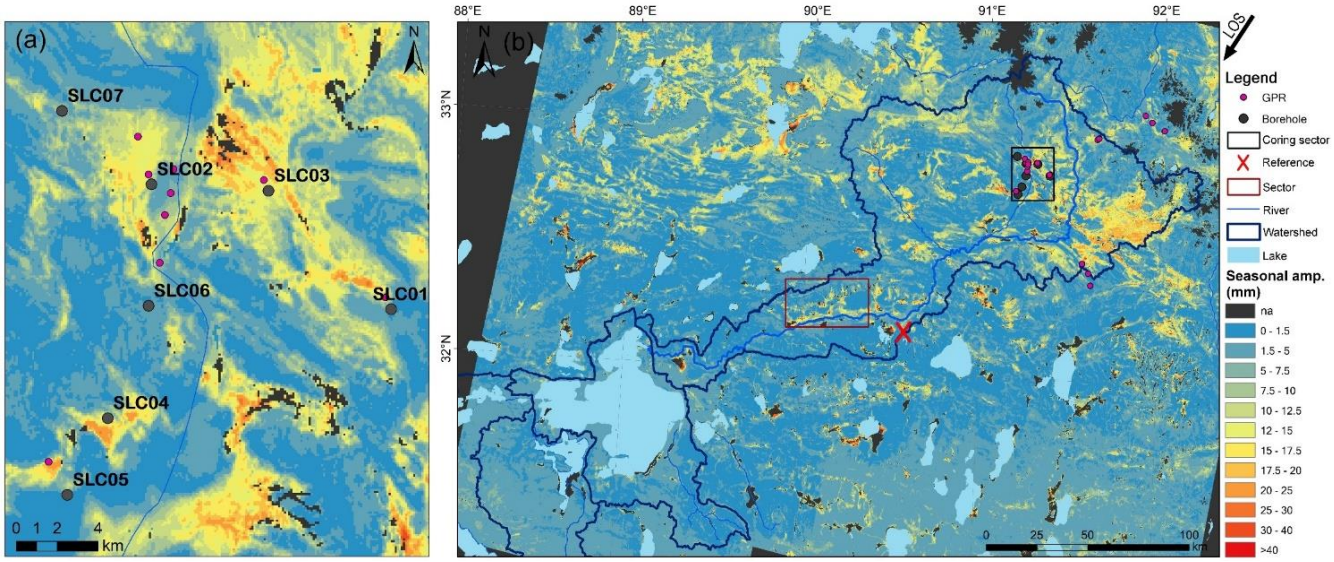

Figure 6 Map of the periodic (seasonal) amplitude in the satellite LOS direction. Subfigure (b) shows an enlarged view of the coring area (black sector in subfigure (a)). Dark grey colored "na" means the information could not be retrieved because of no data or decorrelation.

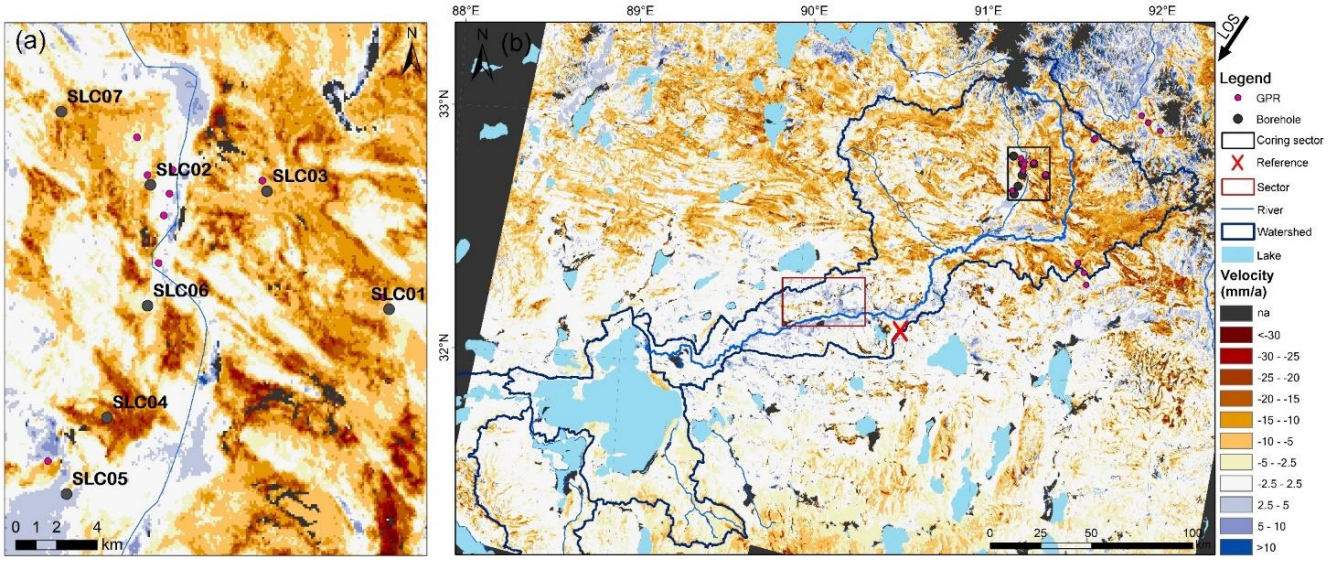

Figure 7 Map of the inter-annual deformation velocity in the satellite LOS direction. Subfigure (b) shows an enlarged view of the coring area (black sector in subfigure (a)). Dark grey colored "na" means the information could not be retrieved because of no data or decorrelation.

The **uncertainty on velocity maps is completely wrong** and should be recomputed or deleted (it is at best of the order of a mm/yr for an evaluation with 100 dates spread over 3 years, and with a reference point located at distance of about 100km). The evaluation cannot be made on smoothed time series unless you consider then temporally correlated noise. It does not then include possible biais or unwrapping error, but that's fair enough.

Thank you for your comment. We have removed this map in the revised manuscript because the uncertainty on velocity is calculated on smoothed time series and doesn't consider the residual errors (unwrapping error, phase ramps, atmospheric distortions). Instead, taking the reviewer's suggestion, we used the network misclosure to evaluate the uncertainties and accuracies of unwrapping error and raw phase time series estimation.

Other comments:

Coring was performed in autumn. Please indicate implication: end of thaw period. Is this why you can conclude from coring that you can measure the depth of the active layer or top of permafrost table? Active layer is by definition evolving through time. Please clarify your methodology here. A sketch of expected permafrost or active layer features with depth would be welcome as I am not sure I really understand the relation between Table 2 permafrost table and "dev of ground ice" columns.

Thank you very much for the comment and suggestion. Yes, from coring, the location of the permafrost table (active layer thickness) and the development of ground ice were described, which provides a sketch of permafrost features. Taking the reviewer's suggestion and to be clear, we have modified the statements as follows, "We conducted a field investigation of the permafrost in the study area in October 2019. Seven boreholes deeper than 20 m were drilled, and ground-penetrating radar (GPR) surveys were carried out in the upstream section of the Zhajiazangbu subbasin (locations are marked in Fig. 1). The survey was performed at the end of the thawing period, allowing us to estimate the maximum thawing depth and the location of the permafrost table. The permafrost table was estimated from the cores of the boreholes, and the development of ground ice was described as well. Descriptions of the boreholes are provided in Table 2, and field photographs of the cores at borehole sites SLC01 and SLC04 are shown in Fig. 2."

Assumption is here done that total settlement is due to ice melting at the top of the permafrost table. Can you discuss a possible contribution of ice/water present in the soil porosity? Would then settlement be less per unit of ice melting, at least in a drained setting?

Thank you very much for the comment. We understand that the reviewer considers that the settlement might be less per unit of ice melting. Based on our experiences from coring in the Selin Co watershed and on the Tibetan Plateau, the permafrost layer just below the permafrost table always contains ground ice higher than 50% in volume (Cheng, 1983; Zhao and Sheng, 2019). So we assumed that the amount of the surface settlement would release the same amount of ground ice caused by compressing the thawing ice-rich permafrost layer. To be clear, we have added these statements in the Introduction section.

Line 372-376: Replace text by a figure showing a density plot of seasonal amplitude versus velocity.

Thank you very much for this suggestion. We have added a density plot in this part as follows. The manuscript states that "Fig. 8 shows a density plot of the seasonal amplitude versus the deformation rate. Subsidence in the Selin Co watershed was normally between 5 and 20 mm/a (see the statistical details in Table 8) but reached 50 mm/a in certain regions, reflecting highly excessive volumes of ice and rapid ice loss in this region. The seasonal amplitude ranged between 0 mm and 60 mm within the watershed area. In the

Zhajiazangbu subbasin with extensive permafrost, among the areas with deformation rates greater than 2.5 mm/a, 0.1% of them had seasonal amplitudes greater than 30 mm, 2.2% had amplitudes between 20 mm and 30 mm, 24.1% had amplitudes between 10 mm and 20 mm, 23% had amplitudes between 5 mm and 10 mm, and 50.6% had amplitudes of less than 5 mm; overall, the average seasonal amplitude was 6.9 mm."

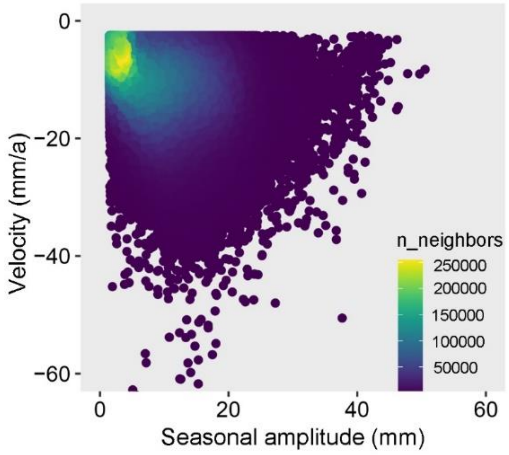

Figure 8 Distribution of the LOS seasonal amplitude versus the LOS deformation velocity within the Selin Co watershed, in all 6.57 ×10^5 valid pixels.

*paragraph 4.2.3: show a zoom of velocity and amplitude map in areas of drillings and GPR, with annotated core numbers

Thank you very much for the suggestion. The zoomed figures of velocity and amplitude in the coring sector have been added in above Fig. 6 and Fig. 7, with the core number annotated.

Appendix Fig. A3 also provides a larger deformation map covering the field investigation region.

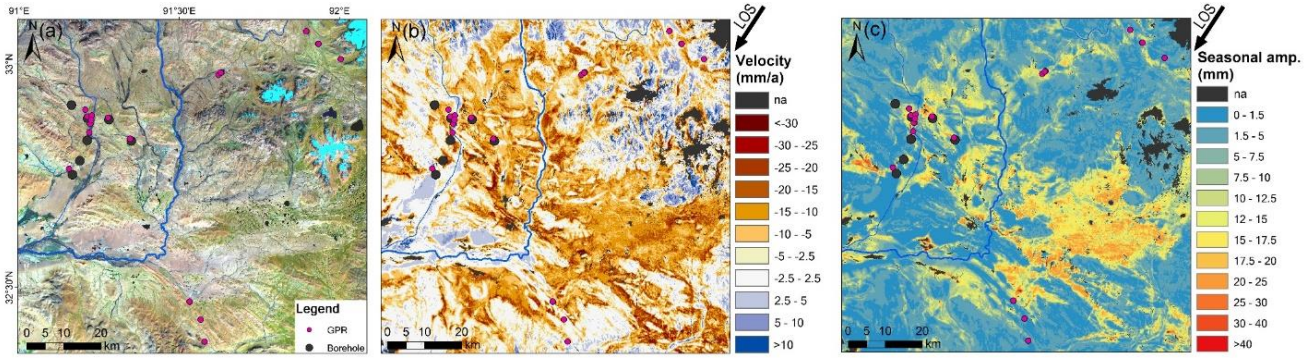

Fig. A3 Maps of the GPR and borehole regions, (a) Landsat 8 image acquired in October 2020 (red: SWIR1, green: NIR, blue: red), with GPR and borehole sites marked, (b) long-term deformation velocity, (c) seasonal deformation amplitude.

Figure 9 : the unit is strange. I suggest to drop the figure as I guess it is simply the velocity multiplied by pixel size. The unit should stay as a velocity as it is a volume per unitsize per unit time.

Thank you for the comment. Yes, it is the vertical velocity multiplied by pixel size, but masked out regions having large slopes and small seasonal amplitude. We agreed with the reviewer that that unit should be velocity. The unit in the figure has been corrected. The figure has been modified and shown as follows.

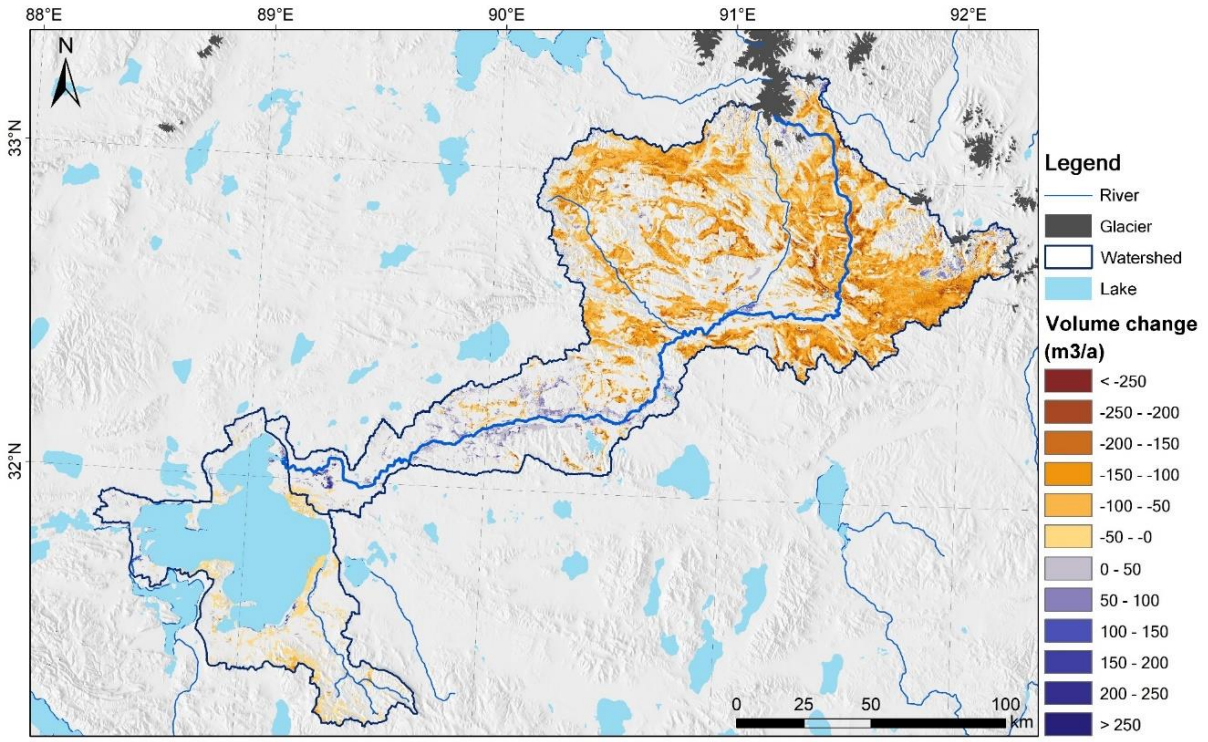

Figure 9 Map of the potential water volume contributed by ground ice melting. The grid color represents the grid cell's yearly groundice meltwater volume, with negative values indicating ground ice loss and meltwater release.

Comments on various parts of the manuscript

The ratio of lake surface to watershed area is about 5.4 %, such that a water level increase of 0.2m/yr corresponds to at least 1cm/a of water collected uniformely over the whole watershed area (neglecting evaporation). With permafrost prone areas covering only a fraction of the watershed (ratio of lake surface to permafrost areas in watershed of 0.18), 4 cm/a of ice melting collected uniformely over the permafrost areas in watershed would be necessary to explain lake level rise. Giving these ratio in the introduction could be useful to the reader to understand the water balance at stake for Serling Co lake.

Thank you very much for the advice. Accordingly, we have modified the statements in Introduction as "The entire Selin Co watershed covers a drainage area of 4.4×10^4 km^2, 18 times the lake surface. Accordingly, a lake water level increase of 0.2 m/a corresponds to at least 1 cm/a of water collected uniformly over the whole watershed area (neglecting evaporation)….according to this permafrost map, the permafrost area covers ~1.3×10^4 km^2, accounting for 30.2% of the watershed. "

To be clear, we have also stated at the beginning of the Abstract that "Selin Co, located within permafrost regions surrounded by glaciers, has exhibited the greatest increase in water storage among all the lakes on the Tibetan Plateau over the last 50 years. Most of the increased lake water volume has been attributed to increased precipitation and the accelerated melting of glacier ice, but these processes are still not sufficient to achieve the water balance with the expansion of Selin Co. Ground ice meltwater released by thawing permafrost due to continuous climate warming over the past several decades was regarded as another source of lake expansion."

Please give a very short description of the permafrost models (extension and ground ice) of Zhao and Sheng 2019 and Zou et al., 2017. I guess it is mostly based on a thermal model and much less on observations. The type of soil is also important: bedrock at the surface cannot host ice I suppose.

Thank you for the suggestion. In the revised manuscript, we have added the statements of permafrost map and ground ice as follows.

"(Zou et al., 2017) mapped the permafrost distribution on the Qinghai-Tibet Plateau (QTP) based on freezing and thawing indices from Moderate Resolution Imaging Spectroradiometer (MODIS) land surface temperatures and validated their map using various ground-based datasets; according to this permafrost map, the permafrost area covers ~1.3×10^4 km^2, accounting for 30.2% of the watershed. Continuous permafrost and seasonally frozen ground exist, with the former being widespread mainly in the northern part of the watershed (Zou et al., 2017). (Zhao and Sheng, 2019) estimated the ground ice storage on the QTP based on the ice content distribution characteristics from 164 drill core records deeper than 15 m, the above permafrost distribution map, a map of the Quaternary sedimentary types, and a permafrost thickness map; based on their map, the ground ice volume in the watershed reaches 132.3 km^3 (Zhao and Sheng, 2019), approximately five times the glacier ice volume in the Selin Co watershed." The 164 drill core records includes along the Qinghai-Tibet engineering corridor, Zhuonai Lake, Altun, West Kunlun Mountains, Gaize, and Wenquan areas), which constructs WE, NS profiles over the Qinghai-Tibet Plateau, and provides the properties of ground ice spatial distribution. The sedimentary type map provides the basic information of soil type.

line 92-93: "long-term subsidence…melting": Please rephrase, not very precise

To be clear, the statement has been rephrased to "we assumed that the amount of surface settlement would release the same amount of ground ice caused by compressing the thawing ice-rich permafrost layer."

Figure 1: enlarge text, numbers, reference point (a cross should be better). Add S-1footprints in a larger area.

Figure 1 has been modified as follows.

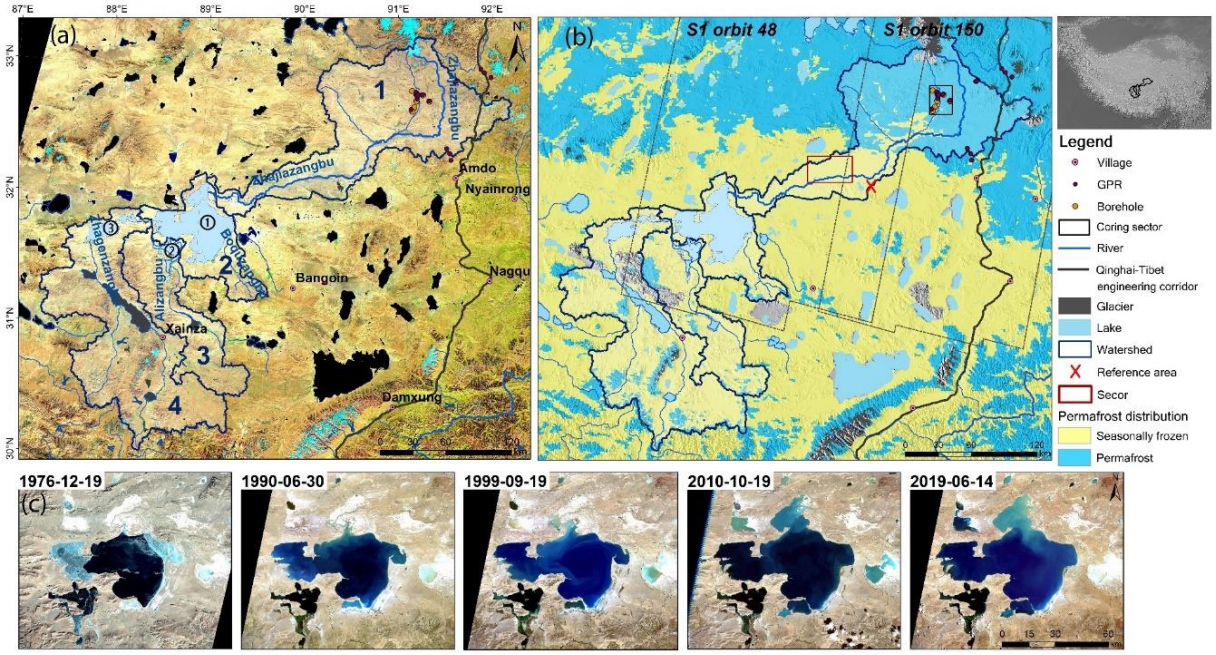

Figure 1 Study area. The base map in Fig. 1(a) is a Landsat 8 image acquired in October 2020 (red: SWIR1, green: NIR, blue: red). The base map in Fig. 1(b) is a permafrost map (Zou et al., 2017); the hillshade is calculated using a 1-arcsec SRTM DEM with the Sentinel-1 incidence angle and azimuth angle. The grey dashed lines delineate two tracks of Sentienl-1 used in this study. The red cross marks the position of our InSAR reference point. The locations of the GPR surveys and boreholes are shown with dots. Fig. 1(c) shows the lake areas from 1976 to 2019 on Landsat optical images.

Table 4 : give date in YYYYMMDD format

The dates in the manuscript have been corrected to the YYYYMMDD format.

line 222: " Every SAR image was coregistered…acquisitions". It is not clear. I guess what is meant is that all interferometric pair processing was done independently from each other (without a stack processing that would result in a stack of co-registered image). It is a bit misleading, so may be rewrite this paragraph starting with explaining that each ifg processing was done independently from each other.

Thank you very much for pointing out this misleading expression. There is stack processing during InSAR processing. To be clear, the sentence has been rewritten as “All the SLC images were coregistered to the stack reference of 20180807 acquisition for orbit 150 and 20180801 acquisition for orbit 48. After generating a coregistered stack of SLC images, interferograms were generated by each SAR image with its two sequential acquisitions.”

line 238: weighting by the inverse of phase variance: variance in space? over what area ? whole interferogram ?

Thank you for the comment. To be clear, the sentence has been rephrased as “During the inversion, interferograms were weighted by the inverse of the phase variance of the whole interferogram (Zhang et al., 2019)..”

The weight matrix takes the form:

$$\mathbf{W} = \mathrm{diag}\left\{1/\sigma^2_{\Delta\varphi^1}, \ldots, 1/\sigma^2_{\Delta\varphi^M}\right\}$$

where $\sigma^2_{\Delta\varphi^j}$ is the phase variance of the j_{th} interferogram calculated through the integration of the phase probability distribution function.

Like minimum cost flow unwrapping method which provides the global optimal result, the weight used here also evaluates the interferogram in global.

line 239: Please cite the other studies that are referenced here

The studies have been cited in the revised manuscript as follows “Different from some studies conducted in permafrost environments that presupposed deformation models to help solve the phase time series (Li et al., 2015; Chen et al., 2018), we did not preset any deformation and instead obtained the raw phase time series by minimizing the phase residual.”

line 271: mosaicking is performed after projection on vertical, so delete here.

Thank you for the comment. During processing, we mosaicked the LOS seasonal amplitude and trend rate

and the incidence angle of two orbits as well. The deformation exhibited throughout the manuscript is in the LOS direction. To be clear, we have modified the sentence in the revised manuscript that “For each orbit, we extracted the LOS periodic (seasonal) amplitude and long-term deformation rate pixel by pixel from the deformation time series and then mosaiced the results from the two orbits together. The spatial grids of the incidence angles from the two orbits were mosaiced as well.”.

line 274 : "Thus, the observed…direction": delete

This sentence has been removed.

line 275: add "assuming no horizontal displacement"

Thank you. It has been rephrased to “For flat terrain, deformation is caused mainly by freeze–thaw cycles within the permafrost layer and occurs predominantly in the vertical direction. Hence, assuming no horizontal displacement, the observed deformation in the line of the sight (LOS) direction was converted into the vertical direction.”

line 288: "long-term…elevation": replace with cumulated settlement

Thank you for the suggestion. It has been corrected.

line 294 /299: if a threshold on velocity, it must be in velocity unit (2.5 mm/yr), so separate thresholds on amplitude and on velocity

Thank you for the suggestion. We’ve stated these two thresholds separately as follows “masking off areas with the LOS direction periodic (seasonal) amplitudes ≤1.5 mm or long-term velocities ≤2.5 mm/a”

line 391: " This sensitivity…SLC04": drop, repetition.

Thank you. Corrected.

line 394: "surface permafrost" : unclear

The surface permafrost in the original manuscript means we don’t consider the situation that the permafrost table is in a very deep place (a few tens of meters). That case is very rare. Thus, it has been replaced with “permafrost” in the revised manuscript to avoid unnecessary misunderstanding.

line 397: SLC03 is repeated twice

Thank you. The second “SLC03” has been deleted.

Fig8: suggestion to put text or symbol or graph of found ice in cores on each panel tofacilitate the reading.

Thank you for the suggestion. We have replotted Fig. 5 and integrated the information on ground ice, and deformation properties (originally listed in Table 7 in the previous manuscript).

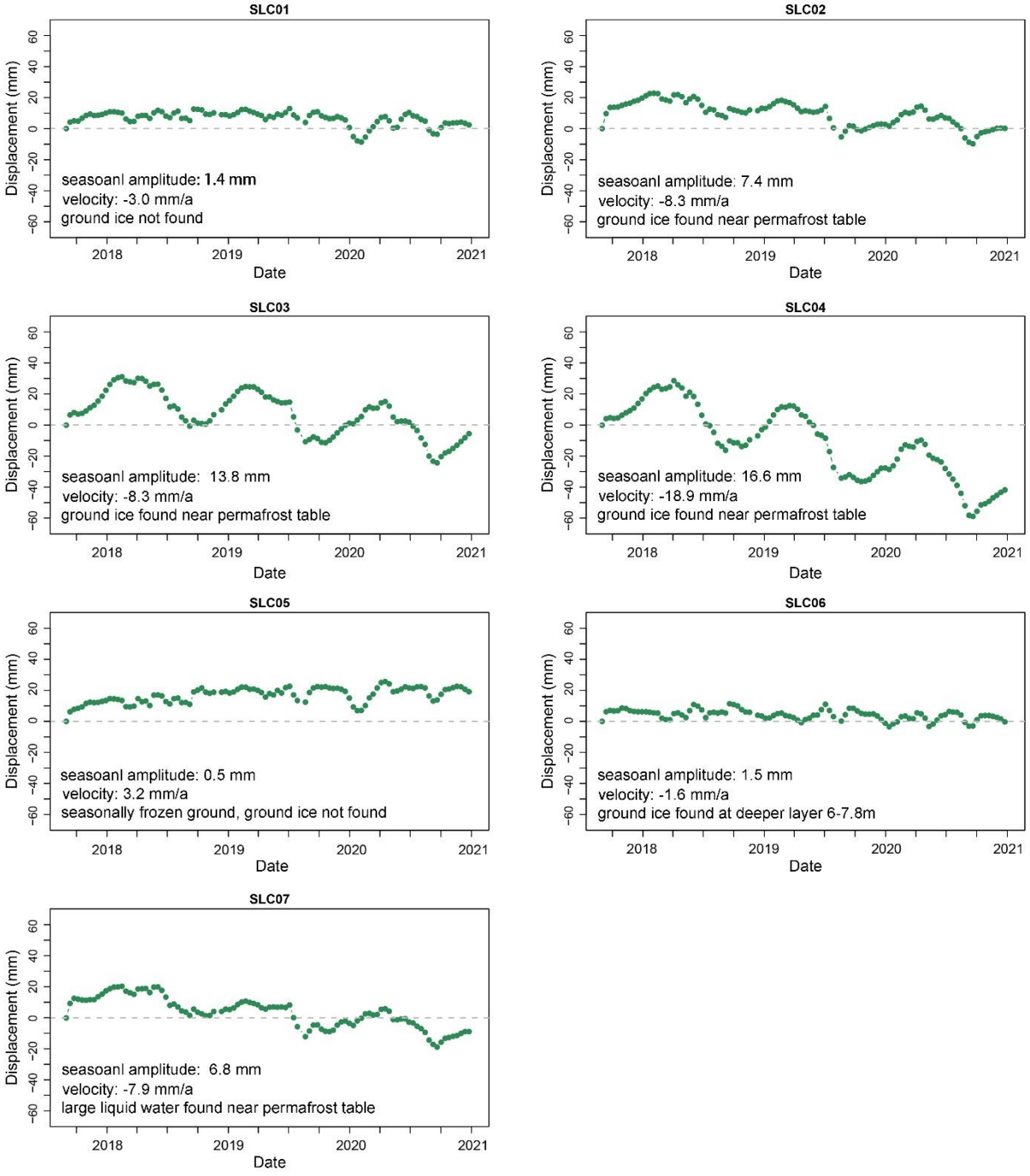

Figure 5 LOS deformation time series at the seven borehole sites. Positive values represent uplift and negative values represent subsidence relative to the first scene of the S1 datasets.

References

Berardino, P., Fornaro, G., Lanari, R., and Sansosti, E.: A new algorithm for surface deformation monitoring based on small baseline differential SAR interferograms, Geoscience and Remote Sensing, IEEE Transactions on, 40, 2375-2383, 2002.

Chen, C. W. and Zebker, H. A.: Phase unwrapping for large SAR interferograms: Statistical segmentation and generalized network models, IEEE Transactions on Geoscience and Remote Sensing, 40, 1709-1719, 2002.

Chen, J., Liu, L., Zhang, T., Cao, B., and Lin, H.: Using persistent scatterer interferometry to map and quantify permafrost thaw subsidence: A case study of Eboling Mountain on the Qinghai-Tibet Plateau, Journal of Geophysical Research: Earth Surface, 123, 2663-2676, 2018.

Cheng, G.: The mechanism of repeated-segregation for the formation of thick layered ground ice, Cold Regions Science and Technology, 8, 57-66, 1983.

Daout, S., Dini, B., Haeberli, W., Doin, M.-P., and Parsons, B.: Ice loss in the Northeastern Tibetan Plateau permafrost as seen by 16 yr of ESA SAR missions, Earth and Planetary Science Letters, 545, 116404, 2020.

French, H. M.: The periglacial environment, John Wiley & Sons2017.

Li, Z., Zhao, R., Hu, J., Wen, L., Feng, G., Zhang, Z., and Wang, Q.: InSAR analysis of surface deformation over permafrost to estimate active layer thickness based on one-dimensional heat transfer model of soils, Scientific reports, 5, 2015.

Pepe, A. and Lanari, R.: On the extension of the minimum cost flow algorithm for phase unwrapping of multitemporal differential SAR interferograms, IEEE Transactions on Geoscience and remote sensing, 44, 2374-2383, 2006.

Zhang, Y., Fattahi, H., and Amelung, F.: Small baseline InSAR time series analysis: Unwrapping error correction and noise reduction, Computers & Geosciences, 133, 104331, 2019.

Zhang, Y., Xie, C., Wu, T., Zhao, L., Wu, J., Wu, X., Li, R., Hu, G., Liu, G., and Wang, W.: New permafrost is forming on the exposed bottom of Zonag Lake on the Qinghai-Tibet Plateau, Science of The Total Environment, 152879, 2022.

Zhao, L. and Sheng, Y.: Permafrost and environment changes on the QinghaiTibetan Plateau (in Chinese), Science Press, Beijing, China2019.

Zou, D., Zhao, L., Yu, S., Chen, J., Hu, G., Wu, T., Wu, J., Xie, C., Wu, X., and Pang, Q.: A new map of permafrost distribution on the Tibetan Plateau, The Cryosphere, 11, 2527, 2017.